LETTER • OPEN ACCESS

Where does the irrigated water in the Tarim Basin go? A hydrological analysis of water budgets and atmospheric transport

ENVIRONMENTAL RESEARCH
LETTERS

LETTER

Where does the irrigated water in the Tarim Basin go? A hydrological analysis of water budgets and atmospheric transport

Jiahui Liu[1], Ting Sun[2,*] and Guangheng Ni[1,*]

[1] State Key Laboratory of Hydroscience and Engineering and Department of Hydraulic Engineering, Tsinghua University, Beijing, People's Republic of China
[2] Institute for Risk and Disaster Reduction, University College London, London, United Kingdom
* Authors to whom any correspondence should be addressed.

E-mail: ting.Sun@ucl.ac.uk and ghni@tsinghua.edu.cn

Keywords: irrigated agriculture, atmospheric hydrological cycle, water resource sustainability, climate, trajectory analysis, WRF

Supplementary material for this article is available online

OPEN ACCESS

RECEIVED
12 January 2023

REVISED
18 February 2023

ACCEPTED FOR PUBLICATION
8 March 2023

PUBLISHED
28 March 2023

Abstract

Irrigated agriculture plays a crucial role in the local economic and social development of the Tarim Basin (TB), but its sustainability is threatened by water scarcity due to the arid environment. In this study, we investigate the impact of irrigation on the atmospheric hydrological cycle in the region using the weather research and forecast model. We conduct simulations for a three month period under two scenarios: present-day and future warming. Our results show that, in the present-day scenario, 90.5% of irrigated water is transported via atmospheric hydrological processes, with precipitation and water vapor transport being the dominant components. However, in the future warming scenario, more atmospheric water (45.2%) will leave the area due to weakened wind regimes, resulting in significant water loss. Furthermore, our analysis using the HYbrid Single Particle Lagrangian Integrated Trajectory model indicates that irrigation contributes to extreme rainfall events, and the southwestern TB is a primary destination for irrigated water. Our findings highlight the urgency of addressing the sustainability of irrigated agriculture and local water resources in the face of impending global warming.

1. Introduction

The Tarim Basin (TB), occupying 44.2% of total agricultural land in northwest China, not only ensures local food security, but also contributes 90% of the country's cotton supply (Xinjiang Bureau of Statistics 2021). Due to the arid nature, more than 95% of the agriculture in TB is sustained by irrigation, which accounts for 92% of the water supply (Xinjiang Bureau of Statistics 2021). Since 2000, the total water resource in TB has been decreasing due to the increase of water consumption; however, the water supply has been increasing (Kadiresan and Khanal 2018, Yang *et al* 2021, Liu *et al* 2021a, 2021c, Monforte and Ragusa 2022), which has raised serious concerns about the sustainability of irrigation-based agriculture in TB (Wei *et al* 2013, Wu *et al* 2015, Zhang *et al* 2016, Bai *et al* 2018, Rosa *et al* 2019).

Irrigation is a key measure to ensure sustainable agriculture—20% of global farmland operated with irrigation produces 40% of global food (Schultz *et al* 2005) but consumes 70% of freshwater supply (Molden 2007, Grafton *et al* 2017, Liu *et al* 2017, Zohaib and Choi 2020). Meanwhile, irrigation is demonstrated to remarkably influence hydro-climate by altering surface energy balance (SEB) and hydrological cycle (McPherson 2007, Biggs *et al* 2008, Sridhar 2013, Yang *et al* 2019): enhanced evaporation can alter SEB by reducing sensible heat fluxes and increasing latent heat fluxes and lead to reduced surface temperature and diurnal temperature range, at both global and regional scales (Haddeland *et al* 2006, Mahmood *et al* 2006, Sacks *et al* 2009, Ozdogan *et al* 2010, Puma and Cook 2010, Sorooshian *et al* 2011, Kueppers and Snyder 2012, Han and Yang 2013, Jiang *et al* 2014, Chen and Dirmeyer 2019); irrigation modifies

the hydrological cycle by increasing soil moisture and surface moisture fluxes, resulting in the increase of the amount of atmospheric water which may indirectly enhance cloud cover and precipitation (Zheng and Eltahir 1998, Boucher *et al* 2004, Gordon *et al* 2005, Mahmood *et al* 2008, Lo and Famiglietti 2013, Tuinenburg *et al* 2014, Lo *et al* 2021). And such influences in precipitation by irrigation are found at both local and regional scales (Segal *et al* 1998, Im *et al* 2013, Phillips *et al* 2022) but through different pathways.

Some studies reveal that the evaporative water vapor added by irrigation directly forms precipitation locally in the irrigated area, increasing the local precipitation recycling rate (Eltahir and Bras 1996, Eltahir 1998, Sorooshian *et al* 2011, Zhang *et al* 2019, Liu *et al* 2021b). At the same time, irrigation may also form a horizontal gradient in the area where the irrigated area and the non-irrigated area overlap, and strengthen the mesoscale circulation, leading to increased precipitation over the non-irrigated area (DeAngelis *et al* 2010, Niyogi *et al* 2010, Guimberteau *et al* 2012, Harding and Snyder 2012a, 2012b, Tuinenburg *et al* 2014, Pei *et al* 2016, Vrese *et al* 2016, Lu *et al* 2017, Nauert and Ancell 2019).

Despite the revealed mechanisms by which irrigation can influence precipitation at different scales around the world, the situation in TB remains elusive. Although increasing trends in greening and precipitation are found in northwest China (Song *et al* 2011, Qiu *et al* 2014, Li *et al* 2015, Ma *et al* 2015, Dong *et al* 2018, Lamchin *et al* 2018, Guan *et al* 2022, Wu *et al* 2022), the role of irrigation in moderating the regional hydrological cycle is yet to be identified. A concerning question in recent study is that if the altered precipitation due to irrigation can support sustainable agricultural development in TB (Xu and Lin 2021). As such, an in-depth study of irrigation on the atmospheric hydrological cycle warrants urgent need in TB.

Concerned about the food security, specifically irrigation sustainability, this study aims to assess the impact of irrigation on atmospheric hydrological cycle and to evaluate the sustainability of irrigation by tracking the irrigated water in different atmospheric processes. In the remainder of this paper, we first describe the modelling techniques (weather research and forecasting (WRF) and HYbrid Single Particle Lagrangian Integrated Trajectory (HYSPLIT)) and their configurations, followed by water balance analysis to reveal the destination of irrigated water in the present-day scenario; we then conduct trajectory analysis to explicate the pathways by which irrigation can influence atmospheric water transport. In addition, we extend the above analysis to a 2050 scenario to understand the potential impacts of irrigation in conjunction with impending global warming on the sustainability of irrigation in TB.

2. Data and methods

2.1. WRF model and configuration

This study employs the WRF model v4.2 (Skamarock *et al* 2019), in which a new irrigation scheme (Valmassoi *et al* 2020) is introduced to allow more detailed operation of irrigation water, to investigate the impacts of irrigation on atmospheric hydrological cycle (Decker *et al* 2017).

For the present-day scenario, the year 2016 is selected as the climate conditions in 2016, specifically the mean air temperature, specific humidity and wind speed, were all located in the 30 year range interval and considered representative of the present climate normal standard (see figure 1 in supplementary material). In addition, the precipitation pattern during the summer of 2016 in the Tarim Basin provides an ideal scenario to examine the impact of irrigation (see figure 3 in supplementary material). The observed lower than multi-year average rainfall in June, and July (12.3 mm and 19.3 mm, respectively, compared to multi-year averages of 23.3 mm and 23.2 mm) could highlight the potential influence of irrigation in comparative simulations between two scenarios in this study. Larger than multi-year average rainfall in August precipitation (77.35 mm vs 25.43 mm) can broaden the scope of the investigation to explore the impact of irrigation on extreme rainfall, which is also key area of interest regarding the regional hydroclimate.

WRF is set up in a one-way nesting mode with two nested domains of 120 × 120 and 240 × 240 grids with resolutions of 15 km and 5 km, respectively: the innermost domain d02 includes the whole TB area and its surrounding mountains (figure 1). The model is configured with 47 sigma levels in the vertical direction with top level set to 50 hPa. Fixed time steps of 30 s and 10 s are set for d01 and d02, respectively. Initial and boundary conditions are provided by the European Centre for Medium-Range Weather Forecasts Reanalysis 5 (ERA5) dataset (Hersbach *et al* 2018) from the European Centre for Medium-Range Weather Forecasts (ECWMF) with a spatial (temporal) resolution of 0.25° (1 h). For more accurate representation of land surface characteristics as of the simulation year (i.e. 2016), global land cover dataset by European Space Agency Climate Change Initiative (ESA-CCI) (European Space Agency 2017) is used to prescribe the land use and land cover in the study area. Besides, albedo, leaf area index (LAI) and vegetation fraction (FVC) are updated using information from Global LAnd Surface Satellite (GLASS) dataset (Liang *et al* 2013a, 2013b, 2021). The simulation is conducted from 00:00 1 May to 23:00 31 August 2016 UTC with the first month as the spin-up period while the remaining three months (June, July and August, or JJA) for analysis. Other physics parameterization schemes used in the simulation are summarized in table 1.

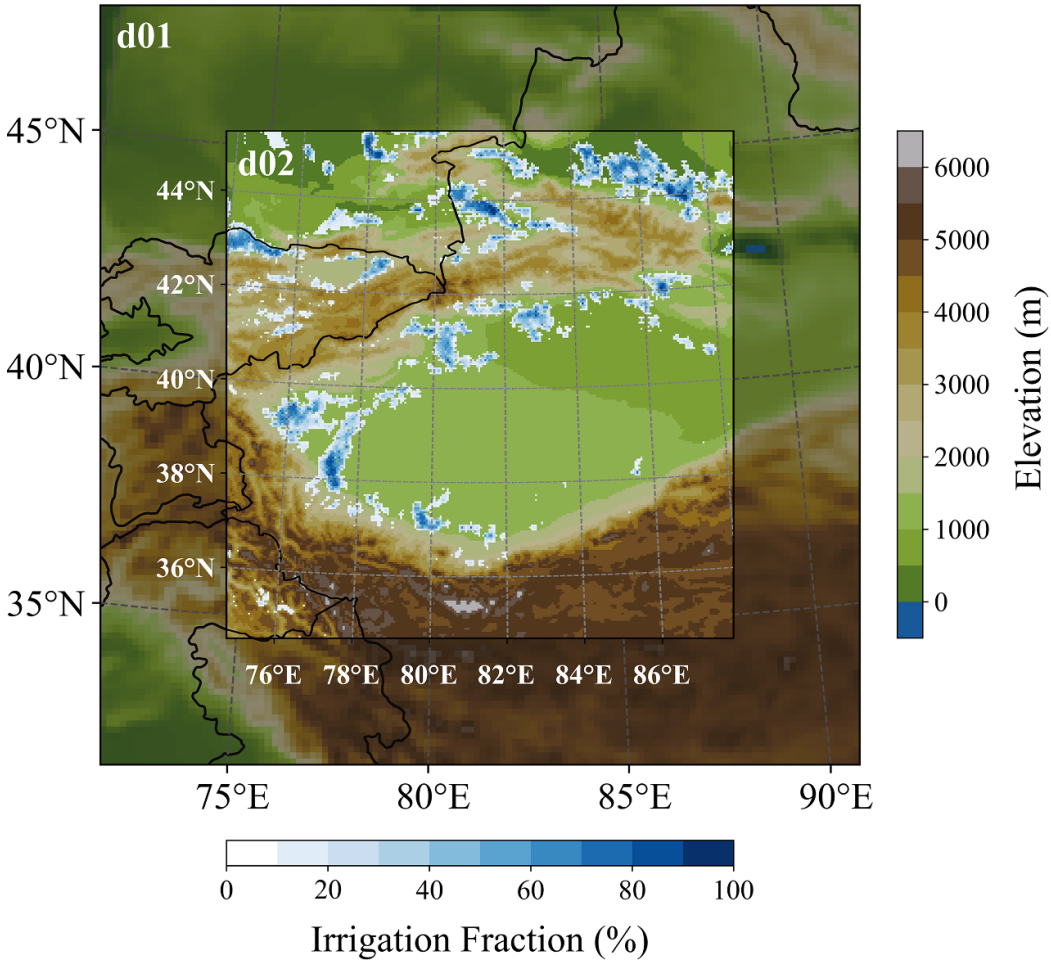

Figure 1. Terrain map of the WRF simulation domain (d01 and d02) covering TB with fractions of irrigated area used in the IRR scenario.

Table 1. Overview of the WRF physics options.

Physics	Scheme	Reference
Microphysics	WSM6	Hong and Lim (2006)
PBL	YSU	Hong *et al* (2006)
Shortwave radiation	RRTMG	Iacono *et al* (2008)
Longwave radiation	RRTMG	Iacono *et al* (2008)
Land surface scheme	Noah LSM	Tewari *et al* (2004)
Surface layer scheme	Monin–Obukhov	Jimenez *et al* (2012)
Cumulus	New Tiedtke Scheme (only for d01)	Zhang and Wang (2017)
Surface irrigation parameterizations	Drip scheme	Valmassoi *et al* (2020)

To assess the effects of irrigation, two scenarios, irrigation (IRR) and default - no irrigation (DFT), are set up for irrigation and default (no irrigation), respectively. For IRR, the irrigation scheme is enabled for the whole simulation area in d02 only during the June, July and August (JJA) period. The amount of irrigation water is set to 6 mm per day according to the local irrigation daily quota (Wu *et al* 2022). In DFT—the benchmark scenario—all surface feature information (land cover, albedo, LAI and FVC) is modified to remove all agriculture-related features (i.e. no irrigated cropland).

For the global warming scenario, the year 2050 is selected as the future timeframe. As the coupled model intercomparison project phase 6 (CMIP6) can forecast future climate up to 2100, 2050 can represent the impending climate in the 21st century (see figure 2 in supplementary material). Meanwhile, 2050, 30 year timeframe, may provide mid-term references for current policy makers. Future meteorological data from bias-corrected CMIP6 global dataset for dynamical downscaling of the Earth's historical and future climate for 2050 under the ssp245 scenario (RCP4.5 global forcing pathway with SSP2 socioeconomic conditions) is used as initial and boundary conditions (Xu *et al* 2021). The dataset is based on 18 models from CMIP6 and ERA5 dataset, provides a state-of-the-art future background climate. Given

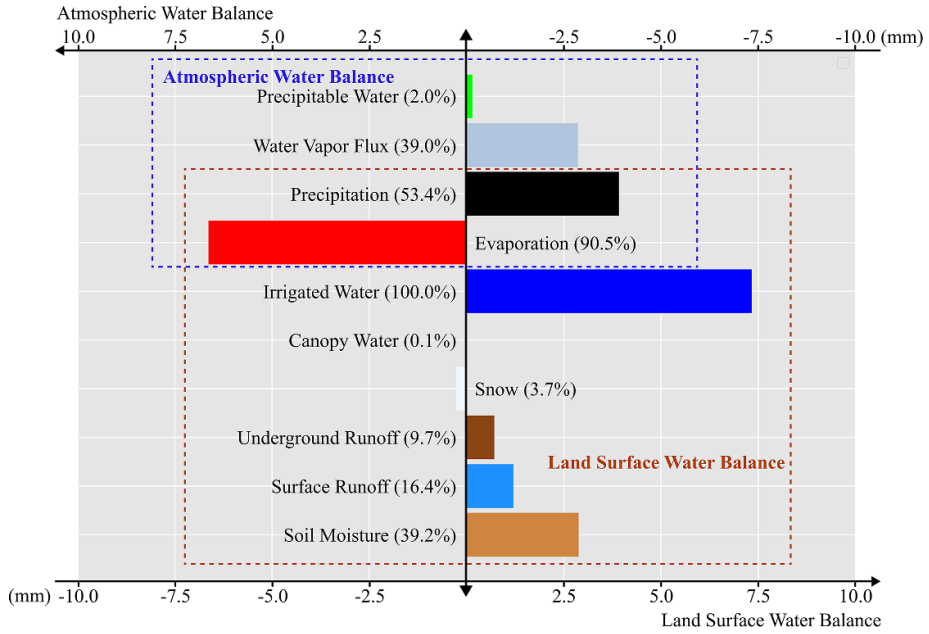

Figure 2. Difference in land surface (brown box) and atmospheric (blue box) water balance budgets between IRR and DFT in 2016. Note: (1) different directions between top and bottom axis; and (2) percentages (in parentheses) for the fractions of irrigated water.

no future projection about the land surface feature information is available in the study area, the present-day land cover information is kept in the 2050 scenario. So that we can give a more straightforward comparison of irrigation impacts between present day climate and global warming. Other settings (e.g. physics parameterization schemes, irrigation settings scenarios, etc) remain the same as the 2016 scenario. In following analysis, all results are based on d02 simulations unless noted otherwise.

2.2. Water balance analysis

To quantify changes in simulated water budgets due to irrigation, we conduct land surface water balance analysis following the equation below:

$$\Delta S = P + I - E - R_S - R_U \tag{1}$$

where ΔS denotes the change in the total storage (including soil water storage ΔSOIL, surface snow storage ΔSNOW and canopy interception ΔCAN), P the precipitation, I the irrigation, E the evapotranspiration, R_S surface runoff and R_U underground runoff. All terms in equation (1) are WRF output variables except for I to be calculated using input information as follows:

$$I = Q_d * D_{JJA} * IF_{avg} \tag{2}$$

where Q_d is the daily irrigation amount (6 mm in this study; see section 2.1), D_{JJA} the number of the JJA days (i.e. 92 days), and IF_{avg} the spatially averaged irrigation fraction of d02 (cf figure 1).

The regional atmospheric water balance is given by:

$$\Delta PW = E - P + \Delta WFT \tag{3}$$

where ΔPW is the change of water vapor content (diagnosed by the WRF-Python tool) while ΔWFT the accumulative water vapor transport on d02 boundaries (note the water vapor content on the model top at 50 hPa is very close to zero). Given the minimal water vapor transport through the top level, we only calculate the vertically integrated moisture flux transport (VIMFT) on four horizontal lateral boundaries as follows (Fasullo and Webster 2003):

$$\Delta WFT = VIMFT_{west} + VIMFT_{east} + VIMFT_{south} + VIMFT_{north} \tag{4}$$

$$VIMFT = -\frac{1}{g}\int_{surface}^{50\ hPa} (q*u + q*v) * dp \tag{5}$$

where g is gravitational acceleration, q the specific humidity at each pressure level, u and v the wind vector.

For both land surface and atmospheric water balance analysis, the differences between IRR and DFT will be calculated later in section 3.1 to reveal the destination of irrigated water. We note that the accumulated water amount for all terms in equations (1) and (2) are averaged over the whole d02 (figure 2), whose corresponding WRF output names (or derivatives using WRF-python) can be found in table 2.

Table 2. WRF output variables used in water balance analysis (cf equations (1), (3) and (5)).

Variables in equations (1), (3) and (5)	Description	WRF output variable
ΔSOIL	Soil Moisture	SMOIS
ΔSNOW	Snow water content	SNOW
ΔCAN	Canopy water content	CANWAT
R_S	Surface runoff	SFROFF
R_U	Underground runoff	UDROFF
P	Precipitation	RAINNC
E	Evaporation	QFLUX
q	Specific humidity	QVAPOR
u	X-wind component	U
v	Y-wind component	V
ΔPW	Precipitable water	pw (diagnosed by WRF-Python (Ladwig2017))

2.3. HYSPLIT-based trajectory analysis

The HYSPLIT model v5.0 (Draxier and Hess 1998, Jiang *et al* 2017, Shi *et al* 2019, Zhang *et al* 2021) is used in this work to compute three-dimensional paths of water vapor particles using wind regimes and topography. Specifically, we use HYSPLIT to calculate backward and forward trajectories of water vapor for the extreme rainfall event peaking on 20 August 2016 (the 820 rainfall event hereinafter) and the transport of irrigation water in July 2016, respectively, for different purposes illustrated below:

(i) The 820 rainfall event: ten day backward trajectories are calculated to trace the origin of rainfall for each hour during the extreme event from 00 UTC 17 to 00 UTC 22 August, 2016 (figure 4). Initial locations are set as the falling area (i.e. accumulated precipitation exceeding 1 mm) of the 820 rainfall event in d02 (32 horizontal locations in figure 5) at 1500 m above ground level. The ten day integration time is chosen because the retention time of moisture in the atmosphere is ten days (Chen *et al* 2012). To identify the main paths from the large number of trajectories, we applied K-means++ cluster method (see Arthur and Vassilvitskii (2007) for details).

(ii) The transport of irrigation water in July 2016: Forward trajectories are calculated to trace the evaporated water vapor from the ground surface over irrigation area for each hour from 00 UTC 1 to 00 UTC 10 July, 2016 without observed rainfall. Initial locations are set as the irrigation area in TB in d02 at 0 m above ground level (97 horizontal locations in figure 6). Integration time is set to 15 day due to minimal residual of air parcels in the atmosphere after a 15 day period.

For both backward and forward trajectory calculations, HYSPLIT uses the hourly wind regime variables from d02 of the IRR scenario as input and produces hourly track points as output.

3. Results and discussion

3.1. Water balance analysis

We first look into the impacts of irrigation on land surface and atmospheric water balance (figure 2). For the surface water balance, the most remarkable change is in the evaporation: 90.5% of irrigated water enters the atmosphere by surface evaporation, leading to the increased precipitation that accounts for 53.4% of irrigated water. As a result of irrigation, the net water amount of land surface is increased: increases are observed in soil moisture (39.2%) and runoff (26.1%) but a slight decrease in the snow water content (−3.7%). While for the atmospheric water balance, in spite of the increased moisture supply from evaporation due to irrigation, the change in atmospheric moisture content is minimal (2.0%). Water vapor transport (39.0%) and precipitation (53.4%) dominate the total atmospheric water content. It is noting that 39.0% of irrigated water is transported out of the domain as water vapor flux. By tracking the hydrological process of irrigated water, the water balance analysis suggests the final destination of irrigated water as the surface water content and water vapor transport. And 90.5% of the irrigated water is transported via the atmospheric hydrological process, in which precipitation (53.4%) and water vapor transport (39.0%) are the two dominant components.

3.2. Impacts on summer precipitation

Remarkable spatiotemporal variability is observed in the precipitation change caused by irrigation (figure 3). The Basin area and the southern mountainous area have seen the largest precipitation increase (figure 3(d)), accounting for 92.8% of the increased precipitation in the domain (59.8% in the basin area and 33.0% in the southern mountain). Although minimal changes are found in the arid basin area during June and July (figures 3(a) and (b)), a large increase in accumulated precipitation is seen in August (figure 3(c)). Outside the basin area, the spatial pattern of precipitation varies during JJA period,

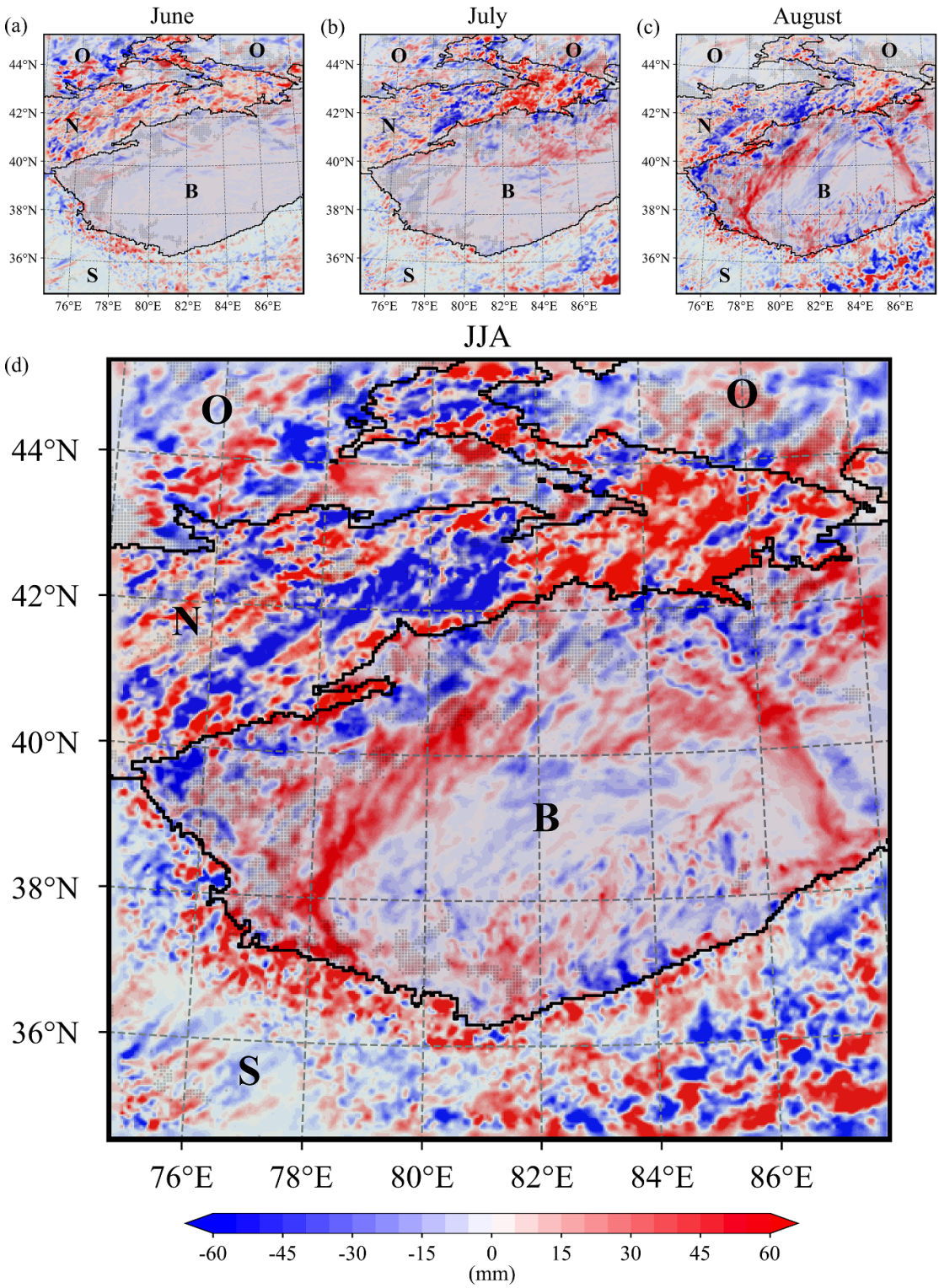

Figure 3. Differences in the accumulated precipitation between IRR and DFT (IRR-DFT) for (a) June, (b) July, (c) August and (d) JJA (cumulated value). Letters indicate different analysis regions: B—Basin area, S—Southern Mountainous area, N—Northern Mountainous area and O—Other areas.

especially in northern mountainous area and other area (cf regions N and O in figures 3(a)–(c)). However, the resultant change in total precipitation is minimal in these two areas (7.2%). So the basin is the most influenced area by irrigation with respect to precipitation, where 59.8% of the total increase is observed.

Given TB (black box shown in figure 4) seeing the largest precipitation increase, we analyze the process of the 820 rainfall event to reveal the detailed influences of irrigation on precipitation. This event occurred in the western TB—adjacent to irrigation area—between 06 UTC 17 August and 21 UTC 21 August. A surge of rainfall was observed from 12 UTC

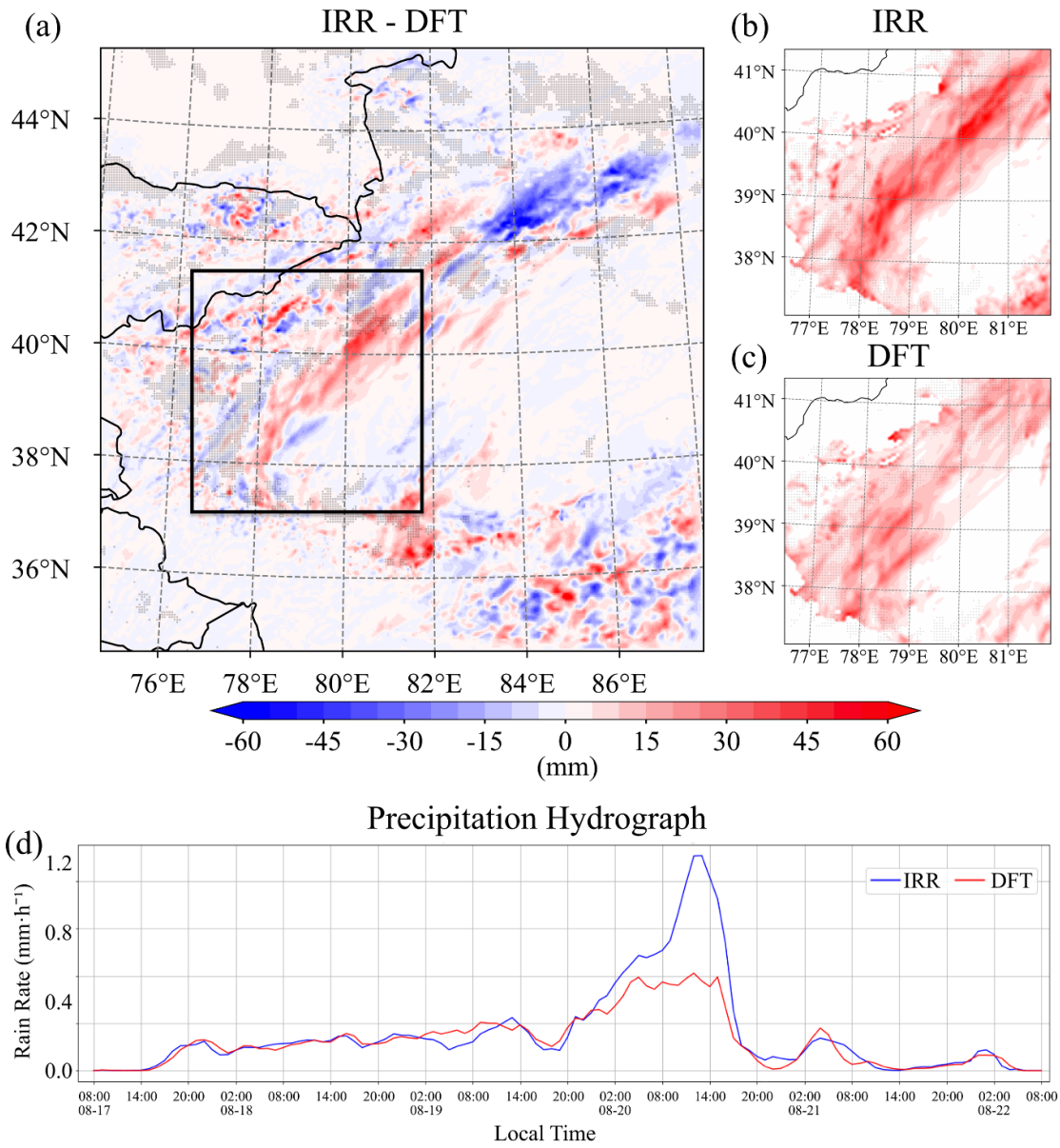

Figure 4. Precipitation during 0000 UTC 17 to 0000 UTC 22 August, 2016 for IRR and DFT: (a) difference (IRR-DFT), (b) accumulation in IRR, (c) accumulation in DFT case, and (d) hydrograph.

19 August to 12 UTC 20 August with peaking rainfall rates of 1.6 mm h^{-1} and 0.8 mm h^{-1} In IRR and DFT, respectively. The ten day HYSPLIT back trajectory analysis (more details see section 2.3) suggests that origin locations of the precipitation are mainly distributed in the interior of TB, in particular the irrigation area at the foot of surrounding mountains (figure 5(a)). We further cluster the back trajectory results to two categories (East cluster and West cluster, accounting for 57.6% and 42.4% of total trajectories, respectively, figures 5(b)–(d)) using the K-means++ method (see Arthur and Vassilvitskii (2007) for details).

For the Eastern cluster (figure 5(c)), the track points are mainly distributed over the irrigation area (red dots in figure 5(c)), and the horizontal distribution is consistent with the contour line, indicating that almost no water vapor comes from outside the mountain area. It is also noting the water vapor source is mainly distributed in the bottom 2000 m of atmosphere (cf coloring of dots in figure 5(c)). Similar distribution of vapour particles is found for the Western cluster (figure 5(d)). So for both Eastern and Western cluster, the irrigated area in TB is the main origin of rainfall water in the 820 event. Compared with DFT, irrigation in IRR strengthens the evaporation process and facilitates precipitation with greater moisture supply. Furthermore, the excessive water vapour supply by irrigation is constrained in the basin due to the sheltering of mountains, which further enhanced the precipitation processes of the 820 rainfall event in IRR scenario. As such, we find that irrigation dominates the precipitation increase in the interior of TB for the 820 rainfall event.

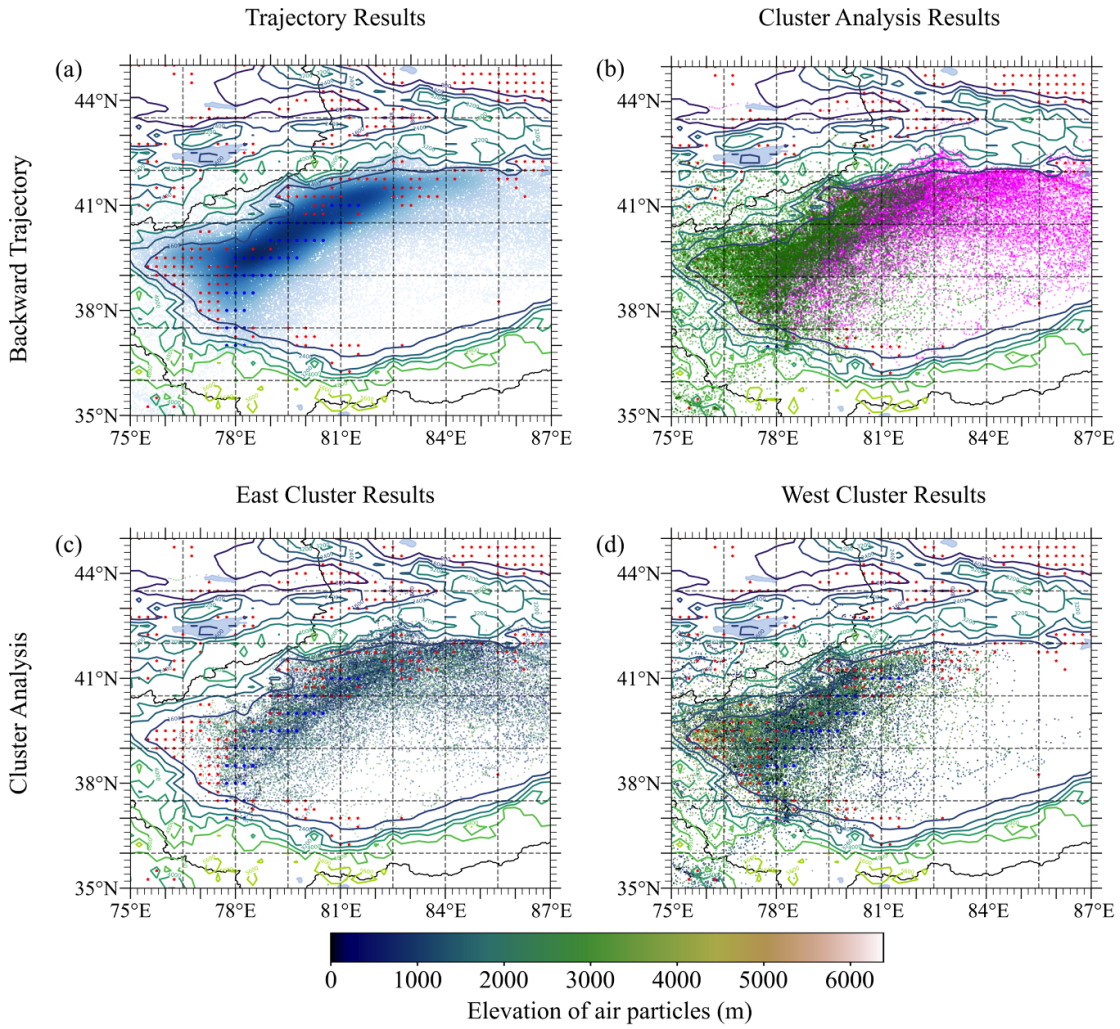

Figure 5. HYSPLIT-based backward trajectory results for the TBP event (a) locations, (b) geographical clustering (purple and green for the east and west clusters, respectively; see section 2.3 for the clustering algorithm) and altitude above ground level (in color bar) for (c) the eastern and (d) western clusters. Red dots indicate the locations of irrigated areas. Colored lines represent topographic contour.

3.3. Impacts on atmospheric water transport

The HYSPLIT forward trajectory analysis is conducted to identify the target area of the irrigated water during a 15 day transportation (configuration details see section 2.3). We analyse the results of northern, western and southern irrigated area for three transportation stages (0–120 h, 120–240 h and 240–360 h). For the northern irrigated area (figures 6(a)–(c)), water vapour particles mainly move to the southwest of the basin along with the dominant north-easterly wind, most of which end in the foothills of the southwestern basin. For the western irrigated area (figures 6(d)–(f)), affected by the downhill wind in the northern and southern mountainous areas, water vapor particles due to irrigation tend to move eastward. However, due to the prevailing north-easterly wind, most of the water vapor particles are transported southward along the basin boundary, where they land close to the mountains—only a small number of particles (0.86%) continue travelling to the eastern boundary. As for the southern irrigation area (figures 6(g)–(i)), the prevailing north-easterly wind could not transport the water vapour particles further southward—outside the basin—due to the blocking of mountains on the southern boundary. In all three areas, most water vapour particles could not travel in the atmosphere longer than ten days—only 8.0% of water vapor particles could. Besides, the height distribution (figures 6(j)–(l)) indicates that the transportation of water vapor is limited to the lower atmosphere (i.e. below 5000 m) with 50.0% and 85.0% under 2000 m and 5000 m, respectively. Putting together all the results from three irrigated areas, we find the southwest of TB is a main destination of water vapor from irrigated areas with notable increase in precipitation (cf section 3.2).

However, given 39.6% of the irrigated water lost via atmospheric water vapor transport from d02 as revealed by the water balance analysis (cf section 2.1), we look into the difference of cumulative water vapor flux on four boundaries between IRR and DFT for causes to understand the destination of the irrigated

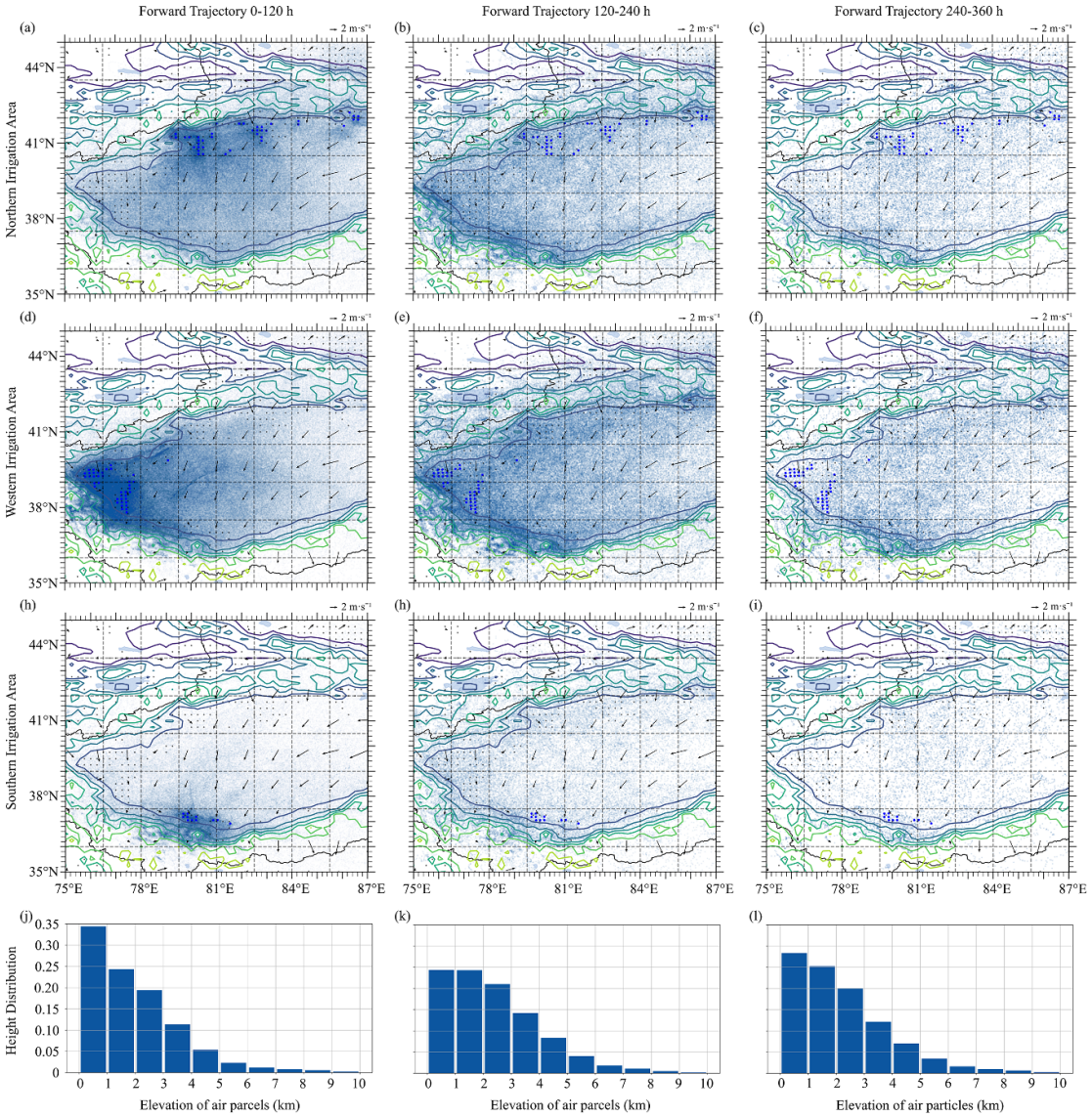

Figure 6. HYSPLIT-based forward trajectory results for the period from 1 July–10 July: locations (left nine subfigures) and height distribution (right three histogram) from three main irrigation areas in three different trajectory periods for 0–5 days (left), 5–10 days (middle), 10–15 days(right). (a)–(c) Horizontal results of northern irrigation area; (d)–(f) horizontal results of western irrigation area; (g)–(i) horizontal results of southern irrigation area; (j)–(l) height distribution in three periods. Blue dots represent locations of irrigation. Colored lines represent topographic contour. The arrow indicates the JJA mean wind speed at 10 m above the ground level.

water in the form of water vapor. By calculating the water vapour fluxes on four horizontal boundaries of d02, we find the eastern boundary the dominant gateway for the loss of water vapor (figure 7(a))—outflow is seen along the mountainous part while inflow in eastern outlet of the basin (cf figure 1), which is due to the water vapor inflow conveyed by prevailing easterly wind. Compared with DFT, the IRR scenario observes less water transported into TB (figure 7(b)), which can also be evidenced by the decreased water vapour flux into the basin (increase in the outflow direction in figure 7(c)). Interestingly, although irrigation has apparently increased the water vapour on the eastern boundary (figure 7(d)), the decreased wind speed in IRR (increase in the outflow direction in figure 7(e)) has reduced the net water vapor transport compared to DFT. Such results suggest irrigation leads to a reduction in the atmospheric water supply on eastern boundary by weakening the prevailing wind. These are consistent with previous findings that irrigation may weaken tropospheric wind speed and atmospheric circulation by the cooling effect (Yeh *et al* 1984, Lee *et al* 2011, Huber *et al* 2014, Shukla *et al* 2014, Yang *et al* 2016, Wu *et al* 2018, Phillips *et al* 2022): irrigation may reduce sensible heating of near-surface atmosphere and enhance evaporative cooling, which can lower the temperature gradient (Kueppers *et al* 2007, Lobell and Bonfils 2008, Lobell *et al* 2009) and thus weaken the atmospheric circulation.

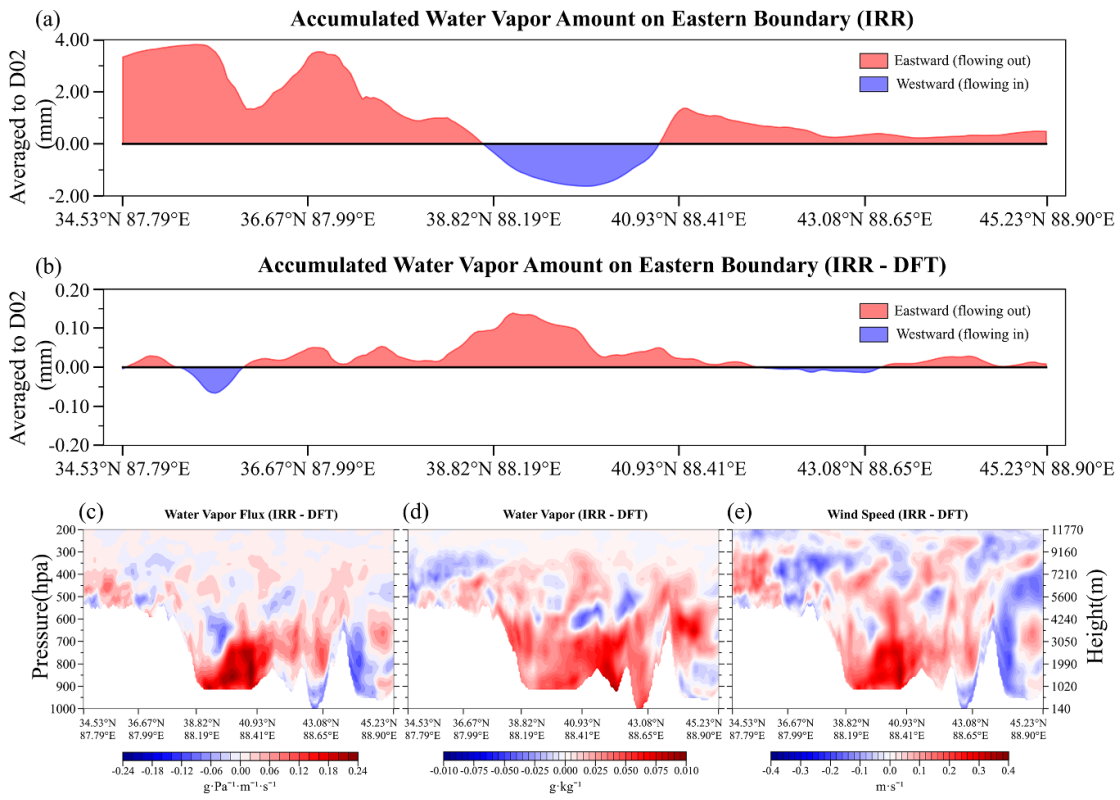

Figure 7. Accumulated water vapor amount for the eastern boundary of the analysis domain (cf figure 1): (a) the IRR scenario, (b) difference between IRR and DFT (i.e. IRR-DFT) and the vertical profiles of: (c) water vapor flux, (d) water vapor and (e) wind speed. Note the coloring indicates the flow direction: red for outflow while blue inflow.

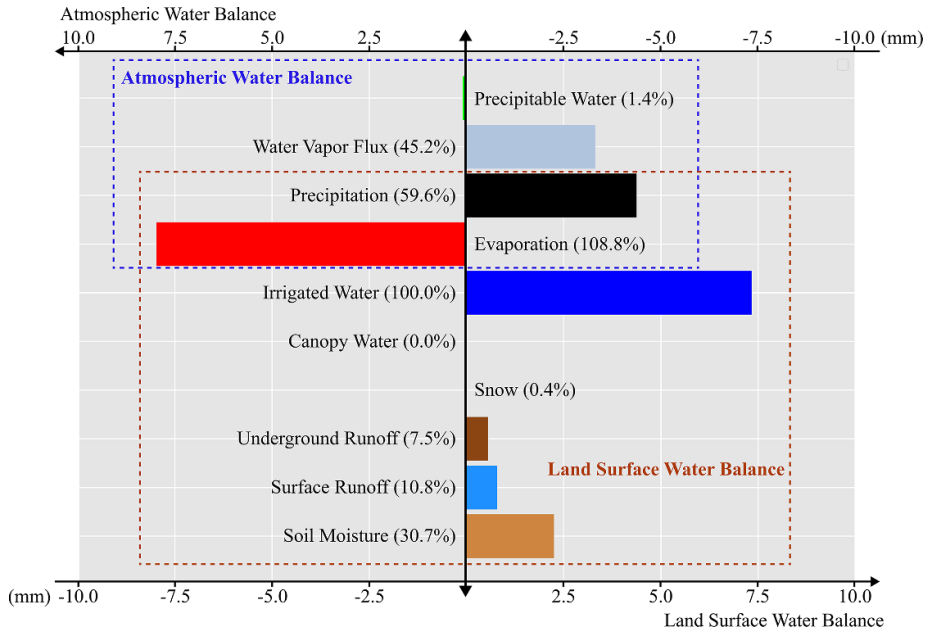

Figure 8. Same as figure 2 but for the future scenario of 2050.

3.4. Implications of global warming

Given the impending global warming, we further look into the future water balance in TB by conducting simulations of the 2050 scenario (details refer to section 2.1) to understand the implications for water resource sustainability. For the surface water balance (brown box in figure 8), in relation to fractions of irrigated water, the evaporation is strongly strengthened under the 2050 scenario to 108.8% (cf 90.5% under the present-day scenario),

the runoff (underground and surface) and soil moisture decrease to 48.6% (cf 61.6% at under the present-day scenario). Both precipitation and water vapor transport processes are enhanced in 2050 (blue box in figure 8): with respect to fraction of irrigated water, the precipitation will increase from 53.4% to 59.6%, while water vapor transport increases from 39.0% to 45.2%, suggesting more water vapor is lost by atmospheric transport. The eastern boundary of the basin is still the dominant gateway for the loss of water vapor in 2050 with notable increase (17.9%) in the atmospheric water loss even without the expansion of agriculture and irrigation.

Putting together the water balance analyses in 2016 and 2050, we conclude that in the context of global warming, irrigation causes stronger evaporation that brings more water to the atmosphere and thus enhances the process of both precipitation and water vapor transport. More water vapor (6.2% of irrigated water) will flow out of the basin than that in 2016. As a result, more attention needs to be paid to the agriculture sustainability and freshwater shortage for the future of TB. With the decrease of both surface and underground water resources and the increase of water supply in Northwest China, the water loss—10.5 billion tonnes, or 1/3 of annual irrigation in Xinjiang (Xinjiang Bureau of Statistics 2021)—caused by irrigation seems to have a negative impact on the sustainable development of agriculture in TB.

4. Conclusion

In this study, we examine the impact of irrigation on atmospheric hydrological cycle in TB by conducting WRF simulations under the present-day and future climate scenarios. The calculation and analysis of surface and atmosphere water balance illustrates the atmospheric transport pathways of the irrigated water. The HYSPLIT model is used to further reveal the destination of the irrigated water and identify the origin of precipitation in the basin. The main findings are summarized as follows:

(i) In the present-day scenario (2016 as the representative year), 90.5% of the irrigated water enters the atmosphere by evapotranspiration. As the result of atmospheric hydrological cycle, 53.4% of the irrigated water goes back to the ground surface by precipitation, and 39.0% leaves the area by atmospheric transport as water vapor. However, in the future scenario (2050 as the representative year), both the evaporation and atmospheric hydrological cycle are enhanced due to global warming, leading to increased loss of irrigated water via atmospheric transport as water (45.2% of 2050 vs. 39.0% of 2016).

(ii) The irrigated water is largely recycled in TB due to the blocking of surrounding mountains, which can be evidenced by both forward and backward trajectory analyses: the forward analysis shows the water vapor from the irrigated area can only be transported to the southwest of the basin by prevailing wind, causing the increase of precipitation in the western part and the southern mountain area to the basin; while the backward trajectory of the precipitation in the basin proves that the origin of the precipitation is the irrigated area.

(iii) Although the irrigation may supply the atmosphere with more water vapor via enhanced evapotranspiration, given the dominant role of external water vapor in replenishing the atmospheric water, the weakening of prevailing wind over the eastern basin boundary lead to a net water loss as a whole. And this situation will be worsened under the future warming scenario: a reduction in atmospheric transport equivalent to 6.2% of irrigated water will be induced by irrigation compared to the present-day value of 39.0%.

Overall, WRF simulations for a three-month period under two scenarios—present-day and future warming—were conducted to examine the impact of irrigation in TB on atmospheric hydrological cycle. In addition, backward HYSPLIT calculation was used to reveal the contributions of irrigation to an extreme rainfall event, and forward HYSPLIT calculation was applied to identify the destination of the irrigated water. By combining WRF simulations and HYSPLIT calculations, this study draws a clear conclusion on the destination of irrigated water in TB. The analysis of current and future scenarios can help policymakers pay more attention to the sustainability of local irrigation water resources. However, we note that only one year irrigation period is simulated, thus the cumulative long-term impact of irrigation still needs to be explored. Besides, this study is focused on the land surface and atmospheric water balance; the impacts on groundwater resources of irrigation warrant future research.

Data availability statement

All datasets used in this study are publicly available from the references indicated. ERA5 data can be requested from cds.climate.copernicus.eu. More information on ESA and GLASS data can be found from www.esa-landcover-cci.org and www.glass.umd.edu, respectively. The data that support the findings of this study are available upon reasonable request from the authors.

Acknowledgments

The study is supported by The National Key Research and Development Program of China (2018YFA0606002), Open Research Fund Program of State Key Laboratory of Hydroscience and Engineering (sklhse-2020-A06), and UKRI NERC Independent Research Fellowship (NE/P018637/2).

ORCID iDs

Jiahui Liu https://orcid.org/0000-0003-2345-5641
Ting Sun https://orcid.org/0000-0002-2486-6146

References

Arthur D and Vassilvitskii S 2007 K-Means++: the advantages of careful seeding *Proc. 18th Annual ACM-SIAM Symp. on Discrete Algorithms (SODA'07)* (New Orleans, LA: Society for Industrial and Applied Mathematics) pp 1027–35

Bai L, Yao K, Yang W, Wang L and Liu H 2018 The Xinjiang production and construction corps family farm land management benefit *IOP Conf. Ser.: Earth Environ. Sci.* **153** 032008

Biggs T W, Scott C A, Gaur A, Venot J-P, Chase T and Lee E 2008 Impacts of irrigation and anthropogenic aerosols on the water balance, heat fluxes and surface temperature in a river basin: irrigation aerosols water heat temperature India *Water Resour. Res.* **44** W12415

Boucher O, Myhre G and Myhre A 2004 Direct human influence of irrigation on atmospheric water vapour and climate *Clim. Dyn.* **22** 597–603

Chen B, Xu X-D, Yang S and Zhang W 2012 On the origin and destination of atmospheric moisture and air mass over the Tibetan Plateau *Theor. Appl. Climatol.* **110** 423–35

Chen L and Dirmeyer P A 2019 Global observed and modelled impacts of irrigation on surface temperature *Int. J. Climatol.* **39** 2587–600

DeAngelis A, Dominguez F, Fan Y, Robock A, Kustu M D and Robinson D 2010 Evidence of enhanced precipitation due to irrigation over the Great Plains of the United States *J. Geophys. Res.: Atmos.* **115** D15115

Decker M, Ma S and Pitman A 2017 Local land-atmosphere feedbacks limit irrigation demand *Environ. Res. Lett.* **12** 054003

Dong W *et al* 2018 Regional disparities in warm season rainfall changes over arid Eastern-Central Asia *Sci. Rep.* **8** 13051

Draxier R and Hess G D 1998 An overview of the HYSPLIT 4 modeling system of trajectories, dispersion and deposition *Aust. Meteorol. Mag.* **47** 295–308

Eltahir E A B 1998 A soil moisture-rainfall feedback mechanism: 1. Theory and observations *Water Resour. Res.* **34** 765–76

Eltahir E A B and Bras R L 1996 Precipitation recycling *Rev. Geophys.* **34** 367–78

European Space Agency 2017 ESA. Land Cover CCI Product User Guide Version 2. Tech. Rep. (available at: maps.elie.ucl.ac.be/CCI/viewer/download/ESACCI-LC-Ph2-PUGv2_2.0.pdf)

Fasullo J and Webster P J 2003 A hydrological definition of Indian Monsoon onset and withdrawal *J. Clim.* **16** 3200–11

Gordon L J, Steffen W, Jönsson B F, Folke C, Falkenmark M and Johannessen Å 2005 Human modification of global water vapor flows from the land surface *Proc. Natl Acad. Sci.* **102** 7612–7

Grafton R Q, Williams J and Jiang Q 2017 Possible pathways and tensions in the food and water nexus *Earth's Future* **5** 449–62

Guan J, Yao J, Li M, Li D and Zheng J 2022 Historical changes and projected trends of extreme climate events in Xinjiang, China *Clim. Dyn.* **59** 1–22

Guimberteau M, Laval K, Perrier A and Polcher J 2012 Global effect of irrigation and its impact on the onset of the Indian summer monsoon *Clim. Dyn.* **39** 1329–48

Haddeland I, Lettenmaier D P and Skaugen T 2006 Effects of irrigation on the water and energy balances of the Colorado and Mekong river basins *J. Hydrol.* **324** 210–23

Han S and Yang Z 2013 Cooling effect of agricultural irrigation over Xinjiang, Northwest China from 1959 to 2006 *Environ. Res. Lett.* **8** 024039

Harding K J and Snyder P K 2012a Modeling the atmospheric response to irrigation in the Great Plains. Part I: general impacts on precipitation and the energy budget *J. Hydrometeorol.* **13** 1667–86

Harding K J and Snyder P K 2012b Modeling the atmospheric response to irrigation in the Great Plains. Part II: the precipitation of irrigated water and changes in precipitation recycling *J. Hydrometeorol.* **13** 1687–703

Hersbach H *et al* 2018 ERA5 hourly data on pressure levels from 1959 to present (Copernicus Climate Change Service (C3S) Climate Data Store (CDS)) (https://doi.org/10.24381/cds.bd0915c6)

Hong S Y and Lim J 2006 The WRF single-moment 6-class microphysics scheme (WSM6) *Korean Meteor. Soc.* **42** 129–51

Hong S-Y, Noh Y and Dudhia J 2006 A new vertical diffusion package with an explicit treatment of entrainment processes *Mon. Weather Rev.* **134** 2318–41

Huber D, Mechem D and Brunsell N 2014 The effects of Great Plains irrigation on the surface energy balance, regional circulation and precipitation *Climate* **2** 103–28

Iacono M J*et al* 2008 Radiative forcing by long-lived greenhouse gases: calculations with the AER radiative transfer models *J. Geophys. Res. Atmos.* **113**

Im E-S, Marcella M P and Eltahir E A B 2013 Impact of potential large-scale irrigation on the West African Monsoon and its dependence on location of irrigated area *J. Clim.* **27** 994–1009

Jiang L, Ma E and Deng X 2014 Impacts of irrigation on the heat fluxes and near-surface temperature in an inland irrigation area of Northern China *Energies* **7** 1300–17

Jiang Z, Jiang S, Shi Y, Liu Z, Li W and Li L 2017 Impact of moisture source variation on decadal-scale changes of precipitation in North China from 1951 to 2010 *J. Geophys. Res.: Atmos.* **122** 600–13

Jiménez P A, Dudhia J, González-Rouco J F, Navarro J, Montávez J P and García-Bustamante E 2012 A revised scheme for the WRF surface layer formulation *Mon. Weather Rev.* **140** 898–918

Kadiresan K and Khanal P R 2018 Rethinking irrigation for global food security: irrigation and food security *Irrig. Drain.* **67** 8–11

Kueppers L M and Snyder M A 2012 Influence of irrigated agriculture on diurnal surface energy and water fluxes, surface climate and atmospheric circulation in California *Clim. Dyn.* **38** 1017–29

Kueppers L M, Snyder M A and Sloan L C 2007 Irrigation cooling effect: regional climate forcing by land-use change *Geophys. Res. Lett.* **34** L03703

Ladwig W 2017 wrf-python (version 1.3.2) (Boulder, CO: UCAR/NCAR) (https://doi.org/10.5065/D6W094P1)

Lamchin M, Lee W-K, Jeon S W, Wang S W, Lim C H, Song C and Sung M 2018 Long-term trend of and correlation between vegetation greenness and climate variables in Asia based on satellite data *MethodsX* **5** 803–7

Lee E, Sacks W J, Chase T N and Foley J A 2011 Simulated impacts of irrigation on the atmospheric circulation over Asia *J. Geophys. Res.: Atmos.* **116** D08114

Li Z, Chen Y, Li W, Deng H and Fang G 2015 Potential impacts of climate change on vegetation dynamics in Central Asia *J. Geophys. Res.: Atmos.* **120** 12345–56

Liang S *et al* 2013b A long-term Global LAnd Surface Satellite (GLASS) dataset for environmental studies *Int. J. Digit. Earth* **6** 5–33

Liang S *et al* 2021 The Global Land Surface Satellite (GLASS) product suite *Bull. Am. Meteorol. Soc.* **102** E323–37
Liang S, Zhang X, Xiao Z, Cheng J, Liu Q and Zhao X 2013a *Global Land Surface Satellite (Glass) Products, Algorithms, Validation and Analysis* (Cham: Springer)
Liu F, Yu Z, Xu E, Li D, Zhang H and Qin Y 2021a Natural and semi-natural land dynamics under water resource change from 1990 to 2015 in the Tarim Basin, China *Environ. Res. Lett.* **16** 085001
Liu G, Wang W, Shao Q, Wei J, Zheng J, Liu B and Chen Z 2021b Simulating the climatic effects of irrigation over China by Using the WRF-Noah model system with mosaic approach *J. Geophys. Res.: Atmos.* **126** e2020JD034428
Liu J, Hertel T W, Lammers R B, Prusevich A, Baldos U L C, Grogan D S and Frolking S 2017 Achieving sustainable irrigation water withdrawals: global impacts on food security and land use *Environ. Res. Lett.* **12** 104009
Liu K, Jiang H and Zhou Q 2021c Spatial analysis of industrial green development and sustainable cities in the Yellow River Basin *Discrete Dyn. Nat. Soc.* **2021** 1–17
Lo M-H, Wey H-W, Im E-S, Tang L I, Anderson R G, Wu R-J, Chien R-Y, Wei J, AghaKouchak A and Wada Y 2021 Intense agricultural irrigation induced contrasting precipitation changes in Saudi Arabia *Environ. Res. Lett.* **16** 064049
Lo M and Famiglietti J S 2013 Irrigation in California's Central Valley strengthens the southwestern U.S. water cycle *Geophys. Res. Lett.* **40** 301–6
Lobell D B and Bonfils C 2008 The effect of irrigation on regional temperatures: a spatial and temporal analysis of trends in California, 1934–2002 *J. Clim.* **21** 2063–71
Lobell D, Bala G, Mirin A, Phillips T, Maxwell R and Rotman D 2009 Regional differences in the influence of irrigation on climate *J. Clim.* **22** 2248–55
Lu Y, Harding K and Kueppers L 2017 Irrigation effects on land-atmosphere coupling strength in the United States *J. Clim.* **30** 3671–85
Ma S, Zhou T, Dai A and Han Z 2015 Observed changes in the distributions of daily precipitation frequency and amount over China from 1960 to 2013 *J. Clim.* **28** 6960–78
Mahmood R, Foster S A, Keeling T, Hubbard K G, Carlson C and Leeper R 2006 Impacts of irrigation on 20th century temperature in the northern Great Plains *Glob. Planet. Change* **54** 1–18
Mahmood R, Hubbard K G, Leeper R D and Foster S A 2008 Increase in near-surface atmospheric moisture content due to land use changes: evidence from the observed dewpoint temperature data *Mon. Weather Rev.* **136** 1554–61
McPherson R A 2007 A review of vegetation-atmosphere interactions and their influences on mesoscale phenomena *Prog. Phys. Geogr.* **31** 261–85
Molden D 2007 Water for food, water for life: a comprehensive assessment of water management in agriculture *Choice Rev. Online* **45** 45-0867
Monforte P and Ragusa M A 2022 Evaluation of bioclimatic discomfort trend in a central area of the Mediterranean Sea *Climate* **10** 146
Nauert C J and Ancell B C 2019 Quantifying the effect of irrigation on nonlocal aspects of the atmosphere *J. Geophys. Res.: Atmos.* **124** 7852–67
Niyogi D, Kishtawal C, Tripathi S and Govindaraju R S 2010 Observational evidence that agricultural intensification and land use change may be reducing the Indian summer monsoon rainfall *Water Resour. Res.* **46** W03533
Ozdogan M, Rodell M, Beaudoing H K and Toll D L 2010 Simulating the effects of irrigation over the United States in a land surface model based on satellite-derived agricultural data *J. Hydrometeorol.* **11** 171–84
Pei L, Moore N, Zhong S, Kendall A D, Gao Z and Hyndman D W 2016 Effects of irrigation on summer precipitation over the United States *J. Clim.* **29** 3541–58
Phillips C E, Nair U S, Mahmood R, Rappin E and Pielke R A 2022 Influence of irrigation on diurnal mesoscale circulations: results from GRAINEX *Geophys. Res. Lett.* **49** e2021GL096822
Puma M J and Cook B I 2010 Effects of irrigation on global climate during the 20th century *J. Geophys. Res.: Atmos.* **115** D16120
Qiu B, Li W, Zhong M, Tang Z and Chen C 2014 Spatiotemporal analysis of vegetation variability and its relationship with climate change in China *Geo-Spatial Inf. Sci.* **17** 170–80
Rosa L, Chiarelli D D, Tu C, Rulli M C and D'Odorico P 2019 Global unsustainable virtual water flows in agricultural trade *Environ. Res. Lett.* **14** 114001
Sacks W J, Cook B I, Buenning N, Levis S and Helkowski J H 2009 Effects of global irrigation on the near-surface climate *Clim. Dyn.* **33** 159–75
Schultz B, Thatte C D and Labhsetwar V K 2005 Irrigation and drainage. Main contributors to global food production *Irrig. Drain.* **54** 263–78
Segal M, Pan Z, Turner R W and Takle E S 1998 On the potential impact of irrigated areas in North America on summer rainfall caused by large-scale systems *J. Appl. Meteorol.* **37** 325–31
Shi Y, Jiang Z, Liu Z and Li L 2019 A Lagrangian analysis of water vapor sources and pathways for precipitations in East China in different stages of the East Asian summer monsoon *J. Clim.* **33** 977–92
Shukla S P, Puma M J and Cook B I 2014 The response of the South Asian summer monsoon circulation to intensified irrigation in global climate model simulations *Clim. Dyn.* **42** 21–36
Skamarock W C, Klemp J B, Dudhia J, Gill D O and Powers J G 2019 A description of the advanced research WRF Version 4 *NCAR Technical Note* NCAR/TN-556+STR (https://doi.org/10.5065/1dfh-6p97)
Song Y, Achberger C and Linderholm H W 2011 Rain-season trends in precipitation and their effect in different climate regions of China during 1961–2008 *Environ. Res. Lett.* **6** 034025
Sorooshian S, Li J, Hsu K and Gao X 2011 How significant is the impact of irrigation on the local hydroclimate in California's Central Valley? Comparison of model results with ground and remote-sensing data *J. Geophys. Res.: Atmos.* **116** D06102
Sridhar V 2013 Tracking the influence of irrigation on land surface fluxes and boundary layer climatology *J. Contemp. Water Res. Educ.* **152** 79–93
Tewari M, Chen F, Wang W, Dudhia J, LeMone M A, Mitchell K, Ek M, Gayno G, Wegiel J and Cuenca R H 2004 Implementation and verification of the unified NOAH land surface model in the WRF model *20th Conf. on Weather Analysis and Forecasting/16th Conf. on Numerical Weather Prediction* pp 11–15
Tuinenburg O A, Hutjes R W A, Stacke T, Wiltshire A and Lucas-Picher P 2014 Effects of irrigation in India on the atmospheric water budget *J. Hydrometeorol.* **15** 1028–50
Valmassoi A, Dudhia J, Sabatino S D and Pilla F 2020 Evaluation of three new surface irrigation parameterizations in the WRF-ARW v3.8.1 model: the Po Valley (Italy) case study *Geosci. Model Dev.* **13** 3179–201
Vrese P, Hagemann S and Claussen M 2016 Asian irrigation, African rain: remote impacts of irrigation *Geophys. Res. Lett.* **43** 3737–45
Wei J, Dirmeyer P A, Wisser D, Bosilovich M G and Mocko D M 2013 Where does the irrigation water go? An estimate of the contribution of irrigation to precipitation using MERRA *J. Hydrometeorol.* **14** 275–89
Wu L, Feng J and Miao W 2018 Simulating the impacts of irrigation and dynamic vegetation over the North China Plain on regional climate *J. Geophys. Res.: Atmos.* **123** 8017–34
Wu L, Feng J, Qin F and Qiu Y 2022 Regional climate effects of irrigation over Central Asia using weather research and forecasting model *J. Geophys. Res.: Atmos.* **127** e2021JD036210

Wu M, Chen Y, Wang H and Sun G 2015 Characteristics of meteorological disasters and their impacts on the agricultural ecosystems in the northwest of China: a case study in Xinjiang *Geoenvironmental Disasters* **2** 3

Xinjiang Bureau of Statistics 2021 *Xinjiang Statistical Yearbook 2021* (Beijing: China Statistical Publishing House)

Xu D and Lin Y 2021 Impacts of irrigation and vegetation growth on summer rainfall in the Taklimakan Desert *Adv. Atmos. Sci.* **38** 1863–72

Xu Z, Han Y, Tam C-Y, Yang Z-L and Fu C 2021 Bias-corrected CMIP6 global dataset for dynamical downscaling of the Earth's historical and future climate (1979–2100) (Science Data Bank) (https://doi.org/10.11922/sciencedb.00487)

Yang B, Zhang Y, Qian Y, Tang J and Liu D 2016 Climatic effects of irrigation over the Huang-Huai-Hai Plain in China simulated by the weather research and forecasting model *J. Geophys. Res.: Atmos.* **121** 2246–64

Yang Y, Liu S, Xiao C, Feng C and Li C 2021 Evaluating cryospheric water withdrawal and virtual water flows in Tarim River Basin of China: an input-output analysis *Sustainability* **13** 7589

Yang Z *et al* 2019 Irrigation impact on water and energy cycle during dry years over the United States using convection-permitting WRF and a dynamical recycling model *J. Geophys. Res.: Atmos.* **124** 11220–41

Yeh T-C, Wetherald R T and Manabe S 1984 The effect of soil moisture on the short-term climate and hydrology change—a numerical experiment *Mon. Weather Rev.* **112** 474–90

Zhang C and Wang Y 2017 Projected future changes of tropical cyclone activity over the Western North and South Pacific in a 20-km-mesh regional climate model *J. Clim.* **30** 5923–41

Zhang C, Tang Q and Chen D 2016 Recent changes in the moisture source of precipitation over the Tibetan Plateau *J. Clim.* **30** 1807–19

Zhang M, Luo G, Cao X, Hamdi R, Li T, Cai P, Ye H and He H 2019 Numerical simulation of the irrigation effects on surface fluxes and local climate in typical mountain-oasis-desert systems in the Central Asia Arid area *J. Geophys. Res.: Atmos.* **124** 12485–506

Zhang S, Liu B, Ren G, Zhou T, Jiang C, Li S and Su B 2021 Moisture sources and paths associated with warm-season precipitation over the Sichuan Basin in southwestern China: climatology and interannual variability *J. Hydrol.* **603** 127019

Zheng X and Eltahir E A B 1998 A soil moisture-rainfall feedback mechanism: 2. Numerical experiments *Water Resour. Res.* **34** 777–85

Zohaib M and Choi M 2020 Satellite-based global-scale irrigation water use and its contemporary trends *Sci. Total Environ.* **714** 136719